Experimental and Analytical Investigation into the Effect of Ballasted Track on the Dynamic Response of Railway Bridges under Moving Loads

Experimental and analytical investigation of the effect of ballasted track on the dynamic response of railway bridges under moving loads

Angelo Aloisio[1], Marco Martino Rosso[2], and Rocco Alaggio[3]

[1]Università degli Studi dell'Aquila, via Giovanni Gronchi n.18, 67100 L'Aquila Email: angelo.aloisio1@graduate.univaq.it

[2]Politecnico di Torino, DISEG, Dipartimento di Ingegneria Strutturale, Edile e Geotecnica Email: marco.rosso@polito.it

[3]Università degli Studi dell'Aquila rocco.alaggio@univaq.it

ABSTRACT

Ballasted tracks are among the most widespread railway track typologies. The ballast possesses multiple functions. Among them, it significantly affects the dynamic interaction between a rail bridge and a moving load in terms of damping and load distribution. These effects entail accurate modelling of the train-track-bridge interaction (TTBI). The paper presents a finite-difference formulation of the TTBI. The governing equations of the track and the bridge, modelled as Euler-Bernoulli (EB) beams, are coupled by a distributed layer of springs representing the ballast. The two equations are solved under a moving load excitation using a Runge–Kutta family algorithm and the finite-difference method for the temporal and spatial discretization, respectively. The authors validated the mathematical model of the TTBI against the displacement response of a rail bridge with a ballasted sub-structure. In a first step, the modal parameters of the bridge, obtained from ambient vibration measurements, are used to estimate the bending stiffness of an equivalent EB beam representative of the tested bridge. In a second step, the authors estimated the coupling effect of the ballast by assessing the model sensitivity to the modelling parameters and optimizing the agreement with the experimental data. Comparing the bridge' experimental displacement responses

highlights the ballast's significant effect on the load distribution and damping. Additionally, optimizing the vertical ballast stiffness and damping provided experimental assessments for predicting TTBI phenomena with the numerical model. The considerable difference between the damping estimated from output-only identification and that determined from the displacement response under moving load proves the dominant role of the ballast in adsorbing the vibrations transmitted to the bridge under the train passage and the different damping sources under high-amplitude excitation. The authors discuss the trade-off between model accuracy and computational effort for a reliable estimation of ballasted tracks response under moving loads.

INTRODUCTION

Ballast is one of the principal components of railway track structures. The components of typical ballasted track structures may be grouped into two main categories, the superstructure (rails, fastening system, sleepers), and the substructure (ballast, sub-ballast subgrade).
Railway ballast is a natural or crushed rock material placed underneath the track superstructure and above the sub-ballast (capping) and subgrade. Standard ballast is a coarse-sized, angular, crushed hard stone and rock uniformly graded, free from dirt and not prone to cementing action. According to (Robnett et al. 1975; Selig and Waters 1994), ballast fulfils multiple functions. The most essential are:

- Retain the track in its required position by opposing vertical, lateral and longitudinal forces applied to the sleepers;
- Provide the required degree of elasticity and dynamic resilience to track superstructure;
- Distribute stresses from the sleeper bearing area to acceptable stress levels for the underlying material;
- Facilitate maintenance surfacing and lining operations (to adjust track geometry) by an ability to rearrange ballast particles with tamping;
- Provide immediate drainage of water falling onto the track;
- Provide sufficient voids for storage of fouling material in the ballast, and to accommodate

the movement of particles through the ballast.

Field measurements and the modal identification of medium spans bridges (Rebelo et al. 2005; Rebelo et al. 2008) showed that the presence of the railway platform, particularly the ballast, significantly affects the boundary conditions and damping of the structure. The dynamic response of railway bridges subjected to moving trains is a popular topic of research in recent years (Xia and Zhang 2005; Frỳba 2013; Yang et al. 2004; Zhai et al. 2013; Xia et al. 2014). Most of the studies focused on the train-bridge interaction modelling (Ribeiro et al. 2012; Majka and Hartnett 2008; Ouyang 2011; Xia et al. 2018; Zhang et al. 2001; Au et al. 2001). For railway bridges, these studies may be generally divided into three categories based on the modelling techniques of trainloads, i.e., the moving load model (Liu et al. 2009; Yang et al. 1997), the moving mass model (Ichikawa et al. 2000; Mao and Lu 2013), and the moving spring-damper system model (Cheng et al. 2001). Parallelly, the studies of railway bridges can be grouped in two categories based on the track modelling. In more complex models, the bridge and the track are represented by 3D finite element (FE) models (Wu et al. 2001; Salcher and Adam 2015; Zhu et al. 2018). Both the bridge and the rack are treated separately and then coupled via a coupling condition at the point of contact (Zhang et al. 2010). Some scholars pursue simplified modelling approaches based on beam-like or shell-like models of the bridge, and the track (Di Lorenzo et al. 2017; Svedholm et al. 2016). The ballast is represented in a simplified manner by spring-damper elements between the track, and the bridge (Das and Luo 2016).

However, which is the trade-off between model complexity in terms of Train-Track-Bridge Interaction (TTBI) and the actual improvement of the experimental data fitting? For instance, Zhang et al. (Zhang et al. 2010) developed an advanced mechanical model of the rail bridge response based on the coupling between two beams representative of the bridge and the track with an elastic bedding representative of the ballasted track. Additionally, the mentioned authors modelled the train as a multidegree of freedom dynamic system. Despite the model complexity, Zhang et al. (Zhang et al. 2010) did not find a satisfactory agreement with the experimental displacement response. There is a high-frequency component in the simulated results not observed in the experimental

data. Additionally, the damping adopted in the calculation, taken as 2% (Xia et al. 2003; Xu et al. 2004; Zhai et al. 2015), significantly underestimates the actual structural damping. Recent papers attempt to generalize the model by further increasing the model complexity. (Hirzinger et al. 2020) developed a non-classically damped beam model on viscoelastic supports crossed by a moving mass-spring system, solved using a dynamic substructuring technique. (König et al. 2021) presents for the first time a semi-analytical approach to analyze the response of a non-classically damped viscoelastic Euler-Bernoulli beam model subjected to a moving mass-spring-damper system.

Still, these papers do not discuss any experimental validation of the presented models, see (Majka and Hartnett 2008). Conversely, other papers on the same topic, like (Feng and Feng 2015), with experimental validation, prove that more simplified models based on the use of beam models for the track and the bridge with viscoelastic coupling, can accurately seize the experimental displacement response with a minor error, compared to more advanced models of the TTBI.

Likely, the growth of the model complexity, the increase of the model parameters to be calibrated can add significant uncertainty to the mathematical model and dramatically increase the computational effort. The higher uncertainty of a sophisticated mathematical model could end in a worse experimental fitting than more elementary approaches. Besides, sophisticated models can only be created with great effort and do not allow parameter studies or stochastic simulations due to the high computational cost.

The authors believe that, at this stage, research is needed for assessing the trade-off between model complexity and model accuracy, rather than further generalizing the mathematical model of the train track bridge interaction by adding additional parameters.

Still, despite the overwhelming number of researches on the dynamic response of bridges under moving loads, a few pieces of research focused on estimating the ballast role using the displacement response of the bridge under moving loads using elementary analytical models and experimental data.

This paper attempts to understand the role of ballast modelling in predicting the bridge response under moving loads. Additionally, the authors attempt to understand whether the modelling of the

train as a sequence of concentrated loads can yield a satisfactory agreement with the experimental data.

The paper presents a finite-difference formulation of the TTBI. The governing equations of the track and the bridge, modelled as Euler-Bernoulli beams, are coupled by a distributed layer of springs representing the ballast. The two equations are solved under a moving load excitation using a Runge–Kutta family and the finite-difference method for the temporal and spatial discretization, respectively. The authors validated the mathematical model of the TBBI against the displacement response of two rail bridges with a ballasted sub-structure. The novel contributions of this article can be summarized as follows:

- Development of a finite difference to evaluate the structural response of a non-classically damped Euler-Bernoulli beam under a moving load excitation
- Validation of the model with the experimental displacement response of a bridge without the ballast under train loads.
- Optimization of the model parameters for assessing the effect of the viscoelastic coupling between the track and the bridge.
- Estimate the structural damping in the two cases and compare the damping estimation obtained from ambient vibration measurements.
- Parametric study on the effect of the train velocity on the response of bridges with and without ballasted tracks.

MATHEMATICAL MODEL OF THE TRAIN-TRACK-BRIDGE INTERACTION (TTBI)

This section describes the mathematical model of the bridge starting from the modelling of the track and the bridge up to the methods followed for the spatial and temporal discretization of the governing differential equations.

Mathematical model of the track

As is well known, the deflection $w_r(x,t)$ of a track with constant mass per unit length $\rho_s A_r$, where ρ_s is the specific mass of steel and A_r is the cross-section area of the rails, and constant

bending rigidity $E_s I_r$, where E_s is the Young's modulus of steel and I_r is the cross-section inertia of the rails, can be described by an Euler-Bernoulli beam model. The equation of motion can be written as: (Di Lorenzo et al. 2017; Kathnelson 1992; Valle et al. 2019)

$$\rho_s A_r \ddot{w}_r(x,t) + E_s I_r w_{r,xxxx}(x,t) = q_r(x,t) + f_r(x,t) \tag{1}$$

where the two dots, $\ddot{w}$, indicate the second time derivative of w, and $w_{r,xxxx}$ is the fourth derivative of w with respect to the spatial coordinate x.

The distributed force $q_r(x,t)$ results from the viscoelastic bedding counteracting the displacement of the track:

$$q_r(x,t) = q_b(x,t) = k_f \left[w_r(x,t) - w_b(x,t)\right] + c_f \left[\dot{w}_r(x,t) - \dot{w}_b(x,t)\right] \tag{2}$$

where k_f and c_f represent the stiffnesss and damping of the viscoelastic Winkler bedding, while w_b is the deflection of the beam representing the bridge substructure. The excitation function $f_r(x,t)$ captures the effect of the interaction forces between the rails and the vehicles.

The train can be modelled by a series of moving concentrated forces with identical intervals, and each car is modeled by a single concentrated force, as shown in Fig.1. The authors assume the train loads are equally spaced instead of considering the exact wheel locations. The legitimacy of this assumption has been confirmed by the satisfactory agreement between experimental and simulated responses. Additionally, the ballast increases the load redistribution, thus endorsing the above assumption. Thus, a train composed of N_v cars can be considered as N_v moving forces, which are numbered as $P_k(1, 2, \ldots, N_v)$. Assuming the first force enters the bridge at the initial time, the time of the k-th load entering the bridge can be expressed as:

$$t_k = (k-1)L_v/c \tag{3}$$

whereL_t is full length of the train and c is the speed of the train.

$$f_r(x,t) = \sum_{k=1}^{N_v} P_k \delta\left[x - c(t - t_k)\right] \tag{4}$$

$$P = \left\{ \frac{P_l}{2}, \left(\frac{P_l}{2} + \frac{P_c}{2} \right), P_c, \ldots, P_c, \ldots, P_c, \frac{P_c}{2} \right\} \tag{5}$$

where L_l is the length of the locomotive, P_k is the concentrated force related to the k-th car, P is the vector collecting all values of P_k. P_c and P_l are loads of the cars and the locomotives. The boundary conditions for a pinned-pinned track can be written as:

$$\text{Left boundary: } w_r(0,t) = 0 \;\; w_{r,xx}(0,t) = 0 \tag{6}$$

$$\text{Right boundary: } w_r(L,t) = 0 \;\; w_{r,xx}(L,t) = 0 \tag{7}$$

where L is the bridge length.

Mathematical model of the bridge

The bridge can be described by Euler–Bernoulli beam. The EB has a constant mass per unit length $(\rho_c A_c + \rho_b A_b)$, where ρ_c is the specific mass of concrete, A_c is the cross-section area of the beam, ρ_b is the specific mass of the ballast and A_b is the cross-section area of the ballasted track, and constant flexural rigidity $E_c I_c$, where E_c is the Young's modulus of concrete and I_c the cross-section inertia of the beam. The vertical displacement $w_b(x,t)$ of the bridge is governed by the following partial differential equation (Frỳba 2013):

$$(\rho_c A_c + \rho_b A_b)\ddot{w}_b(x,t) + E_c I_c w_{r,xxxx}(x,t) = q_b(x,t) \tag{8}$$

The boundary conditions for a pinned-pinned track can be written as:

$$\text{Left boundary: } w_r(0,t) = 0 \;\; w_{r,xx}(0,t) = 0 \tag{9}$$

172

173 $$\text{Right boundary: } w_r(L,t) = 0 \;\; w_{r,xx}(L,t) = 0 \tag{10}$$

174 **Spatial discretization**

175 The equations of motion of the bridge–soil and the track subsystems can be written in matrix
176 form as:

177 $$\begin{aligned}\begin{bmatrix} (\rho_c A_c + \rho_b A_b) & 0 \\ 0 & \rho_s A_r \end{bmatrix} \begin{Bmatrix} \ddot{w}_b(x,t) \\ \ddot{w}_r(x,t) \end{Bmatrix} + \begin{bmatrix} E_c I_c & 0 \\ 0 & E_s I_r \end{bmatrix} \begin{Bmatrix} w_{b,xxxx}(x,t) \\ \ddot{w}_{r,xxxx}(x,t) \end{Bmatrix} + \\ + \begin{bmatrix} -k_f & k_f \\ k_f & -k_f \end{bmatrix} \begin{Bmatrix} w_b(x,t) \\ w_r(x,t) \end{Bmatrix} + \begin{bmatrix} -c_f & c_f \\ c_f & -c_f \end{bmatrix} \begin{Bmatrix} \dot{w}_b(x,t) \\ \dot{w}_r(x,t) \end{Bmatrix} + \begin{Bmatrix} 0 \\ f_r \end{Bmatrix}\end{aligned} \tag{11}$$

178 Fig.2 illustrates the mathematical model of the TTBI. The spatial discretization is obtained using
179 the finite difference method, by approximating the fourth derivative with the approximate fourth
180 derivative matrix. The beam is divided into n elements with a Δx length. The two coupled partial
181 derivative equations in Eq.11 can be discretized into the following:

182 $$\begin{aligned}\begin{bmatrix} (\rho_c A_c + \rho_b A_b)\Delta x \boldsymbol{I} & \boldsymbol{0} \\ \boldsymbol{0} & \rho_s A_r \Delta x \boldsymbol{I} \end{bmatrix} \begin{Bmatrix} \ddot{\boldsymbol{w}}_b(t) \\ \ddot{\boldsymbol{w}}_r(t) \end{Bmatrix} + \begin{bmatrix} E_c I_c \boldsymbol{D}_4 - k_f \Delta x \boldsymbol{I} & k_f \Delta x \boldsymbol{I} \\ k_f \Delta x \boldsymbol{I} & E_s I_r \boldsymbol{D}_4 - k_f \Delta x \boldsymbol{I} \end{bmatrix} \begin{Bmatrix} \boldsymbol{w}_b(t) \\ \boldsymbol{w}_r(t) \end{Bmatrix} + \\ + \begin{bmatrix} -c_f \Delta x \boldsymbol{I} & c_f \Delta x \boldsymbol{I} \\ c_f \Delta x \boldsymbol{I} & -c_f \Delta x \boldsymbol{I} \end{bmatrix} \begin{Bmatrix} \dot{\boldsymbol{w}}_b(t) \\ \dot{\boldsymbol{w}}_r(t) \end{Bmatrix} + \begin{Bmatrix} 0 \\ \boldsymbol{f}_r \end{Bmatrix} = 0\end{aligned} \tag{12}$$

183 where $\boldsymbol{I}^{\{n\times n\}}$, $\boldsymbol{0}^{\{n\times n\}}$ are the identity and null matrices, $\boldsymbol{D}_4^{\{n\times n\}}$ is the approximate fourth matrix
184 derivative defined in Eq.30, $\boldsymbol{w}_b(t)^{\{n\times 1\}}$ and $\boldsymbol{w}_r(t)^{\{n\times 1\}}$ collect the vertical deflection of the bridge
185 and track models discretized in N segments, $\boldsymbol{f}_r^{\{n\times 1\}}$ discretizes the moving force vector described
186 in Eq.1.

187 Matrix $\boldsymbol{D}_4^{\{n\times n\}}$ must satisfy the boundary conditions. Appendix A details all the algebraic passages
188 needed for the assemblage of the fourth derivative matrix, which satisfies the boundary conditions
189 of a simply supported beam.

190 Eq.12 can be re-written using the conventional notation for multi-degrees of freedom dynamic

systems:

$$\boldsymbol{M}\ddot{\boldsymbol{x}}(t) + \boldsymbol{C}\dot{\boldsymbol{x}}(t) + \boldsymbol{K}\boldsymbol{x}(t) = \boldsymbol{f}(t) \tag{13}$$

where $\boldsymbol{M}^{\{2n\times 2n\}}$, $\boldsymbol{C}^{\{2n\times 2n\}}$ and $\boldsymbol{K}^{\{2n\times 2n\}}$ are the mass, damping and stiffness matrices, while $\boldsymbol{f}(t)$ is the forcing term. The displacement vector has the following definition: $\boldsymbol{x}^{\{2n\times 1\}} = \{\boldsymbol{w}_b(t)^{\{n\times 1\}}, \boldsymbol{w}_r(t)^{\{n\times 1\}}\}$.

Temporal discretization

The temporal discretization requires the formulation of Eq.13 into the state space. The continuous-time state space model of Eq.13 can be written in the classical form:

$$\dot{\boldsymbol{x}}(t) = \boldsymbol{A}(t)\boldsymbol{x}(t) + \boldsymbol{B}\boldsymbol{u}(t) \tag{14}$$

where $\boldsymbol{x}(t)$, $\boldsymbol{A}(t)$ and $\boldsymbol{B}$ and $\boldsymbol{u}(t)$ are defined after (Craig Jr and Kurdila 2006) using the mass $\boldsymbol{M}^{\{2n\times 2n\}}$, damping $\boldsymbol{C}^{\{2n\times 2n\}}$ and stiffness $\boldsymbol{K}^{\{2n\times 2n\}}$ matrices, and the forcing term $\boldsymbol{f}(t)^{\{2n\times 1\}}$.
Eq.14 is then transformed in the following discrete form using Tustin Approximation method (Åström and Wittenmark 2013):

$$\dot{\boldsymbol{x}}_k = \boldsymbol{A}_k\boldsymbol{x}_k + \boldsymbol{B}\boldsymbol{u}_k \tag{15}$$

where k indicates the time step. Eq.15 is solved using the Dormand-Prince method based on an explicit Runge-Kutta temporal discretization (Dormand and Prince 1980).
As supplementary material of this reseach paper, the authors provided the Matlab code written used for estimating the approximate solution of Eq.15.

CASE STUDY: BRIDGE WITH A BALLASTED TRACK

The considered bridge is in the Orte-Falconara railway line, in the municipality of Trevi (Italy).

Bridge description

The viaduct consists of 46 spans of about 20 m lengths, see Fig.3. Each span is a structure of 8 pre-tensioned beams equipped with four crosspieces with rectangular cross-sections. The planimetric route of the piers identifies a curve with a radius equal to about 2232 m.

Fig.4 details the cross-section of each span. The beams are 1.40 m high. The upper and lower wings are 1.20 m and 0.70 m wide, respectively. The eight beams have a shear reinforcement by the supports. Therefore the thickness of the core of the beam varies from 16 to 33cm. The prestressing reinforcement is arranged in the lower wing, and, according to the design drawings of the time, it consists of 29 cables arranged in 3 rows, sheathed at the support. The crosspieces are also prefabricated and are therefore born integral with the beam. They have a rectangular cross-section with a 40cm width and a height equal to the beams. There is a 20 cm thick reinforced concrete slab with 1.40 cantilevered elements, which support the side walkways to the railway line and the parapets. The total width of the deck is about 12.40 m and bears two running tracks. Tab.3 lists the geometrical characteristics of the bridge cross-section. The typical pile consists of a pseudo-rectangular reinforced concrete wall (with maximum dimensions equal to 11.0 x 1.50 m). The pulvinus has the same shape as the pile, with plan dimensions higher than 30 cm and an average height equal to 50 cm. The foundation of the piles consists of a 2 m high reinforced concrete plinth, with plant dimensions of 5.60 x 12.80 m, sustained by 8 piles with a 1.20m diameter. The abutments are made up of reinforced concrete cantilever walls 1.10 m thick.

Dynamic identification

The experimental layout consists in two rows of seven equally-spaced Force Balance Accelerometers (FBA) (Aloisio et al. 2020b; Aloisio et al. 2020a). The two extreme accelerometers were placed by the supports with a mutual spacing equal to 3.3m. The accelerometers were arranged into two measurement chains, each one driven by a master recording unit connected to a Wi-Fi access point and synchronized by GPS receivers, see Fig.5. The dynamic tests were carried out under ambient excitation. The time series are about 20 minutes long. The modal parameters are estimated using the covariance-driven Stochastic Subspace Identification (SSI) method (Peeters and De Roeck 2001).

The data were sampled at a rate of 200 Hz. The cut-off frequency of the anti-aliasing filter was set to 40 Hz. The preprocessed data were used for SSI and subsequent modal analysis, resulting

in eigenfrequencies, damping ratios, mode shapes and covariances of these modal parameters for each setup. The parameters used for the identification are $i = 7$, $n = 20$ and $n_b = 70$ (Reynders et al. 2008). The first bending and torsional modes are at approximately 8 and 9Hz, see Fig.6. The higher modes mainly involve the deformation of the wings and are not discussed in the this research.

Deterministic updating of the beam model

The outcomes from dynamic identification proved that the bridge exhibits both bending and torsional modes. However, the bending modes are not coupled with the torsional ones. Specifically, the first mode closely resembles that of a pinned-pinned beam. The modal components by the supports are almost null, proving that the bearing deformation can be considered negligible in the current case study. Additionally, the modal components associated with the two rows of accelerometers are almost coincident, proving prevalent bending rather than torsional modal deformation (Aloisio et al. 2021c). Therefore, the first bending mode in terms of mode shapes and natural frequencies can be reasonably used to estimate the bending stiffness EI_b of an equivalent beam model. The natural frequencies and mode shapes of a pinned-pinned EB beam are:

$$f_n = \left(\frac{n^2\pi}{2L^2}\right)\sqrt{\frac{EI_b}{\rho A_b}} \quad \phi_n = \sin\left(\frac{n\pi}{L}x\right) \tag{16}$$

where n id the mode number, f_n the n-th natural frequency, ϕ_n the n-th mode shape.

The authors solved the following nonlinear least-squares problem: (Mottershead et al. 2011; He et al. 2021):

$$\hat{\boldsymbol{\theta}} = \arg\min_{\boldsymbol{\theta}} J(\boldsymbol{\theta}) = \arg\min_{\boldsymbol{\theta}} \sum_i w_{\epsilon,i} \left(\epsilon_{z,i}(\boldsymbol{\theta})\right)^2 \tag{17}$$

where $\epsilon_{z,i}$ denotes the residuals between the experimental and numerical modal data z. Herein, only the undamped eigenvalue $z = \lambda$ is involved by considering $\lambda_i = (2\pi f_i)^2$

$$\epsilon_{\lambda_i}(\boldsymbol{\theta}) = \frac{\lambda_i(\boldsymbol{\theta}) - \tilde{\lambda}_i}{\tilde{\lambda}_i} | i \in \{1 - n\} \tag{18}$$

where the upper tilde denotes the experimental values and f stands for the natural frequency. In Eq.(25), $w_{\epsilon,i}$ is the weighting factor. Herein, we assumed $w_{\epsilon,i} = 1$.

Fig.7 shows that the global minimum of the objective function corresponds to an $EI_b \approx 126000$kN/mm, using the parameters in Tab.3 to estimate the mass per unit of length.

EXPERIMENTAL TESTS

The experimental equipment consisted of two easels supporting a laser sensor. The laser sensors are Micro-epsilon optoNCDT 1420. The sampling rate is 1000Hz. The C-Box/2A controller (Micro-epsilon) synchronizes and digitizes the two signals, which are acquired by a personal computer from an Ethernet cable. A lead-acid battery provides power to both the laser sensors, the controller and the personal computer. The two lasers measured the displacement response of 3rd and 6th beam intrados. Fig.8 shows the experimental setup for the Orte-Falconara bridge.

Fig.8 shows the experimental displacement response of the bridge under four different moving trains. In the following sections, the measurement No 4 has been selected for the sensitivity analysis due to knowledge of the train weight, which can be assumed. In the other train passages, the authors have no precise knowledge of the weight and geometric characteristics of the train. The inspection of the experimental data may suggest the following comments:

- **Damping**. There are no free oscillations as the train exits the bridge. Theoretical and experimental evidence proved that free oscillations can occur after the train passage, see (Frỳba 2013). Likely, the lack of free oscillations depends on the high-damping of the ballasted track.
- **Load distribution**. The displacement response is the superposition of two components. One is almost quasistatic, the other oscillatory. This effect is evident in Train No 1, when the spacing between the train axes is lower than the beam length. However, this effect is also manifest in the other plots, where the spacing between the train axes equal to 22m is larger than the beam length. Theoretically, if there is no load redistribution and the train behaves like a concentrated load, the beam should return to the non-deformed configuration

after the train passage. Nevertheless, there is a minor beam deflection when the train has exited the beam, possibly due to the load redistribution effect of the ballast, which spreads the concentrated load to a broader influence area.

- **Rotational response**. The train loads are eccentric and cause an evident torsional response. The authors are modelling the bridge like an EB beam. Therefore, they purged the response from the torsional response by extracting the mean value, also shown in Fig.9.
- **Displacement Peaks** The difference between the peak displacement values, especially between the first or last and the central ones, depend on the weight difference between the locomotives and the cars.

SENSITIVITY ANALYSIS

Before estimating the values of the modelling parameters associated with the optimal agreement with the experimental data, a covariance-based sensitivity analysis provided a quantitative assessment of their effect on the rank correlation coefficient and the peak displacement response. Following (Gibbons 1985; Aloisio et al. 2021a), the rank correlation coefficient can be used to estimate the degree of similarity between the experimental $\boldsymbol{x}_m$ and simulated $\boldsymbol{x}_s$ displacement response. The correlation is defined as:

$$\text{corr}(\boldsymbol{x}_s, \boldsymbol{x}_m) = \frac{\boldsymbol{x}_s \cdot \boldsymbol{x}_m}{|\boldsymbol{x}_s| \cdot |\boldsymbol{x}_m|} \tag{19}$$

where $(\cdot)$ is the inner product and $|\ |$ the norm operator. The authors chose the following parameters for the sensitivity analysis: the parameters of the ballast, the bending stiffness of the beam and the train velocity. Tab.2 lists the parameters and their range of variation.

The vertical stiffness of the ballast ranges between 6 and 600 MPa. The lower bound is obtained by assuming an estimate of the Winkler coefficient for compacted gravel (c_{gravel}):

$$k_{f,\text{lower}} = c_{\text{gravel}} \cdot \frac{B}{2} = 10^6 [\text{kN/m}^3] \cdot 6.2 \approx 6 \cdot 10^6 = 6\text{MPa} \tag{20}$$

where B is the span width. The upper bound is obtained by assuming a hundred times the lower

bound. The ballast can be very stiff, and there is no consensus on the possible ranges of variation of its vertical deformability.

$$k_{f,\text{upper}} = k_{f,\text{lower}} \cdot 100 = 600\text{MPa} \tag{21}$$

Therefore, the authors chose to consider a broad but consistent interval.

It is also doubting to provide a reasonable range of variation for the nonproportional damping coefficient (c_f). Some trial tests compared the response associated with a nonproportional damping coefficient and an equivalent damping ratio, assuming that the damping matrix is proportional to the mass and stiffness matrices. Eqs.22-23 show the correspondence between the nonproportional damping coefficient c_f and the equivalent damping ratio ξ_{eq}:

$$c_{f,\text{lower}} \approx 0.1\text{Mpa}/s \rightarrow \xi_{eq} \approx 10‰ \tag{22}$$

$$c_{f,\text{upper}} \approx 20\text{Mpa}/s \rightarrow \xi_{eq} \approx 200‰ \tag{23}$$

The equivalent damping ratio is estimated by minimizing the squared error between the maximum displacement response modelled as non proportional damping and using an equivalent viscous damping coefficient following (Aloisio et al. 2021b). The upper bound might seem an exaggerated overestimation of damping. However, as shown in the following paragraphs, the damping in ballasted tracks under the train transit is considerable and may result in super-critical damping. The lower and upper bounds of the bending stiffness are obtained by lowering or increasing the optimum bending stiffness found from deterministic model updating using the first experimental natural frequency. The train velocity ranged between 30 and 200 km/h, which are velocity limits in specific railway trails.

The sensitivity analysis is limited to the parameters in Tab.2 because the goal is assessing the effect of the modelling choices. The authors seek the following answers: Is the ballast's contribution significant?; is it possible to achieve an engineering model by neglecting the ballast and considering

the sole beam bending stiffness?; Is the load velocity a high-sensitive parameter?. In conclusion, the analysis would declare the error in adopting the simplest mechanical model, a beam with a static load representative of the moving train axis, neglecting the effect of velocity and ballast. Tab.3 lists the input parameters, assumed as known in the sensitivity analysis. Fig.10 shows qualitative plots indicating the effect of the chosen parameters on the displacement response.

- **Effect of** k_f: The vertical stiffness of the ballast affects both the amplitude of the response and the delay between train transit and beam deflection. If the vertical stiffness is lower, the train behaves like a concentrated load, while a higher vertical stiffness determines a significant load distribution and lower displacement values.
- **Effect of** c_f: The authors show the displacement response using the equivalent viscous damping to assess the damping effect qualitatively. If the damping is very low, $\xi_{eq} \approx 20‰$, there is a significant growth in the amplitude of the response. Additionally, the oscillations tend to be symmetric to the undeformed configuration. Higher damping is associated with a higher reduction of the displacement response after the first oscillation. Therefore, the succession of the different train loads does not allow the beam to oscillate, whose response almost corresponds to a quasi-static loading. Besides, it is also manifest that high damping is not associated with significant free-oscillations occurring in the experimental data after the end of the trainloads.
- **Effect of** EI: The bending stiffness has the sole effect of amplifying or reducing the displacement response by a specific scaling factor. It has no significant impact on the delay between the load application and the beam deflection.
- **Effect of** c: The train velocity mainly affects the displacement amplitude and, obviously, the duration of the time series. Therefore, the velocity variation has been eliminated in the sensitivity analysis of the rank correlation coefficient.

Fig.10 proved that the chosen parameters have a significant effect on the displacement response. Therefore, the authors carried out a systematic covariance-based sensitivity analysis. The multi-

variate sensitivity analysis allows decomposing the variance of the output (objective function, and peak displacement) of the model into fractions which can be attributed to the chosen parameters (Pasca et al. 2021). The first step is setting the inputs sampling range (Tab.2) and generate the model inputs according to the Saltelli's sampling scheme (Saltelli and Sobol' 1995). ($N \cdot (2D + 2)$ model inputs were generated, where $N = 100$ is the number of samples, and $D = 4$ is the number of input parameters).

After running all the model inputs the first-order (S_1) and total-order (S_T) sensitivity indices were calculated. S_1 and S_T measure respectively, the effect of varying a single parameter alone and the contribution to the output variance of the selected parameter including all variance caused by its interactions with the other parameters.

Tab.4 lists the values of the sensitivity indicators in two separate analyses. The first focused on the sensitivity to the peak displacement of the k_f, c_f, EI and c. The latter evaluated the sensitivity of the rank correlation coefficient to k_f, c_f, EI.

k_f and EI manifest the most significant influences. The S_1 and S_t coefficients attain approximately 40% in both analyses. The damping coefficient of the ballast is also determinant, with sensitivity indicators close to 20%. The train velocity has a minor effect compared to the other parameters. This fact is confirmed by several literature findings, as remarked by (Frỳba 2013).

The closeness between the first-order and total-order proves that the chosen parameters are substantially uncorrelated. Therefore, they can be used for global optimization without the risk of solving an overdetermined problem.

OPTIMIZATION OF THE MODEL PARAMETERS

The experimental displacement data are used to calibrate the stiffness and damping parameters of the ballasted track. The calibration was performed by using a genetic optimization algorithm (Pelliciari et al. 2018; Sirotti et al. 2021). The genetic algorithm performs iteration of parameters with the goal of minimizing the following objective function: The parameters which yield the

maximum correlation in Eq.21 are chosen as optimum parameters:

$$\hat{\boldsymbol{X}} = \arg\min_{\boldsymbol{X}} \operatorname{corr}(\boldsymbol{d}_{s,s}, \boldsymbol{d}_{s,m}) \tag{24}$$

$$\operatorname{obj}(\mathbf{p}) = \frac{\sum_{i=1}^{N} \left| \left[w_{b,ei} - w_{b,si}(\mathbf{p}) \right] \Delta t_i \right|}{\sum_{i=1}^{N} \left| w_{b,ei} \Delta t_i \right|} \tag{25}$$

where N is the number of data points, $\mathbf{p}$ is the parameter vector containing the ballasted track parameters, $w_{b,ei}$ and Δt_i are the experimental deflection of the bridge, and $w_{si}(\mathbf{p})$ is the simulated beam deflection. Note that the objective function is defined as normalized integral of the difference between experimental and simulated displacement. This gives a measure of discrepancy between experimental data and model simulation. The optimization was carried out by defining the lower and upper bounds for the model parameters displayed in Tab.2.

As anticipated in the previous sections, the authors assumed the value of the bending stiffness EI_{opt} in Tab.1 to further constrain the optimization problem. Differently from (Feng and Feng 2015), the train speed is not included in the updating, being estimated from the video recording of the train passage. Tab.3 reports the additional geometric and mechanical parameters used in the calculation. The weight of the train is known in the sole passage No 4, plotted in Fig.9. Therefore, the optimization is limited to the mentioned displacement record.

$$\boldsymbol{p} = \{k_f, c_f\} = \{490.49 \text{ Mpa}, 14.50 \text{ Mpa} \cdot s\} \tag{26}$$

Eq.26 shows the parameters obtained from the global optimization, while Fig.11 superposes the experimental and simulated displacement response associated with the optimized parameters. The comparison is very satisfactory. The displacement peaks are almost corresponding. Additionally, the oscillations damp after each train load, as observed in the experimental data. The optimum value of k_f is almost 80 times the expected value for compacted gravel. Additionally, c_f close to 14 Mpa·s is associated to an equivalent damping ratio close to 100%. To the authors' knowledge, there are no experimental estimates for k_f and c_f based on the model updating of the experimental dis-

placement response. (Feng and Feng 2015) achieved an excellent agreement with the experimental displacement by using an EB beam without the ballast and focused the optimization to the bending stiffness. The mentioned research paper presents the results of a sensitivity analysis of k_f and c_f to the train velocity, but it does not provide an estimate using the experimental data. Therefore, the authors cannot provide a comparison with experimental estimates from the scientific literature.

Fig.12 illustrates the qualitative effects of different damping values. Damping mainly affects the amplitude of oscillation after the exit of the train load. Damping does not affect the dominant frequency f_{dominant} of the response arises which depends from repeated trainloads (Ju et al. 2009):

$$f_{\text{dominant}} = \frac{nc}{L_v} \tag{27}$$

where n is the order of the dominant frequency.

EFFECT OF THE TRAIN VELOCITY ON THE BRIDGE RESPONSE

The authors carried out a parametric analysis to verify the effect of velocity on the displacement amplification. The dynamic amplification factor has the following definition:

$$A = \frac{v_{\text{max}}}{v_{\text{max,static}}} \tag{28}$$

where A is the dynamic amplification factor, v_{max} is the maximum value of the absolute displacement and $v_{\text{max,static}}$ is the maximum displacement under an almost static load (c =30km/h). The velocity is varied in the range 5-1500 km/h to observe the all trend of the dynamic amplification curve. Fig.13 plots the dynamic amplification factor versus the adimensional velocity α and the equivalent viscous damping. The adimensional velocity has the following definition:

$$\alpha = \frac{f_{\text{dominant}}}{f_1} \tag{29}$$

where f_{dominant} is defined Eq.27, and f_1 is the first natural frequency of the bridge. As remarked by several scholars (Frỳba 2013), the dynamic amplification factor in railway bridges is close to unit

and generally below 2.

The TTBI does not modify this result. The dynamic amplification factor is below 1.15 also in case of lighter damping. The maximum amplification occurs when the frequency of excitation (f_{dominant}) approximately equals the first natural frequency of the bridge. The amplification corresponding to $\alpha \approx 1$ vanishes in case of higher damping. There is no amplification if the equivalent viscous damping is close to one. Conversely, the amplification factor reduces as the adimensional velocity grows if the equivalent viscous damping exceeds the critical damping.

Interestingly, the amplification curve associated with lower damping values is erratic, exhibiting local maxima and minima. This phenomenon is not a flaw of the time integration but depends on the so-called cancellation phenomenon.

Several pieces of research observed that the free vibrations of a uniform beam generated by a single moving load are maximum (local) at some velocities and of zero amplitude at some others (cancellation speeds), as reported (Museros et al. 2013; Pesterev et al. 2003; Xia et al. 2014). This phenomenon depends on the interaction between the excitation frequency and the modal parameters of the bridge, causing the free-response cancellation after the load transit. This effect determines a reduction of the inertial effects, as proved in Fig.13. The cancellation points are infinite and grow in density as they approach zero. The first cancellation point, as estimated by (Kumar et al. 2015), occurs if the adimensional velocity equals 0.33. This is evident in Fig.13, where the curve for $\xi_{eq} = 0.2$ is one for $\alpha \approx 0.31$. The effects associated with other cancellation points are minor and not evident from Fig.13, because the amplification factor is already very close to unity. The effects of cancellation are not evident in the case of higher damping values.

Despite the arising of local maxima due to cancellation effects, the influence of amplification on the maximum bridge displacement is negligible. Both research papers and technical guidelines confirm this aspect. Additionally, realistic values of the train velocity ($c < 300$km/h) do not allow an appreciation of a significant dependence of the amplification factor on the train velocity. Still, despite the A factor not being a crucial parameter in design, the experimental estimation of the A-α curve can be used to identify the damping with higher accuracy. In conclusion, the TTBI does

not appreciably affect the dynamic amplification factor, as estimated from more elementary models based on the simulation of a beam with moving concentrated loads (Frỳba 2013).

CONCLUSIONS

The paper presents a mathematical model of the Train-Track-Bridge interaction (TTBI) based on the coupling between two Euler-Bernoulli beams representing the track and the bridge and a distributed layer of springs and dashpots representative of the ballast.

Several authors developed complex mathematical models of the TTBI without experimental validation. Additionally, the few researchers who attempt to use the experimental data to update the TTBI model propose more straightforward approaches by focusing on the bending stiffness optimization (Feng and Feng 2015). Which is the trade-off between model complexity and accuracy? Although a significant accuracy can be achieved by neglecting TTBI, the modelling of the TTBI can simulate peculiar effects related to the ballast, manifest from experimental data: the high damping and load re-distribution associated with a ballasted track.

The authors selected a prestressed concrete rail bridge as a case study. The mid-span displacement response recorded under a train passage is used to optimize the mechanical characteristics of the ballasted track.

In the first step, the operational modal analysis of the bride and the estimation of the first natural frequency is used to determine the bending stiffness of the bridge by assuming an estimate of the mass per unit of length. The bending stiffness estimation aims to constrain further the optimization of the mechanical properties of the ballast. A variance-based sensitivity analysis of the peak displacement response and the rank correlation coefficient proves that the bending stiffness and the mechanical properties of the ballast similarly affect the displacement response. Furthermore, qualitative plots proved how different values of the bending stiffness and characteristic of the ballast modify the shape and amplitude of the estimated mid-span displacement. A higher stiffness of the ballast causes a higher load distribution and a lower displacement value. Conversely, higher damping reduces the oscillations after the succession of the trainloads so that the displacement response possess almost the same sign, as confirmed by the experimental data. In a second step, after

assuming reasonable estimates of the bounds of the parameters, a genetic optimization algorithm is used to find the optimum agreement with the experimental data. The obtained values for the vertical stiffness and non-proportional damping of the ballast are approximately equal to 400Mpa and 14 Mpa·s. To the author's knowledge, no researches show estimates of the two parameters for further validation. As the last task, the authors assessed the effect of velocity on the peak displacement response. Future research applications will aim at assessing whether the modelling of the trainload as a mass-spring-damper system is beneficial for a more reliable prediction or is only an undesirable source of uncertainty.

DATA AVAILABILITY STATEMENT

All data, model and code that support the findings of this study are available from the corresponding author upon reasonable request.

REFERENCES

Aloisio, A., Alaggio, R., and Fragiacomo, M. (2020a). "Dynamic identification and model updating of full-scale concrete box girders based on the experimental torsional response." *Construction and Building Materials*, 264, 120146.

Aloisio, A., Alaggio, R., and Fragiacomo, M. (2020b). "Time-domain identification of elastic modulus of simply supported box girders under moving loads: method and full-scale validation." *Engineering Structures*.

Aloisio, A., Alaggio, R., and Fragiacomo, M. (2021a). "Bending stiffness identification of simply supported girders using an instrumented vehicle: Full scale tests, sensitivity analysis, and discussion." *Journal of Bridge Engineering*, 26(1), 04020115.

Aloisio, A., Alaggio, R., and Fragiacomo, M. (2021b). "Equivalent viscous damping of cross-laminated timber structural archetypes." *Journal of Structural Engineering*, 147(4), 04021012.

Aloisio, A., Pasca, D. P., Alaggio, R., and Fragiacomo, M. (2021c). "Bayesian estimate of the elastic modulus of concrete box girders from dynamic identification: A statistical framework for the a24 motorway in italy." *Structure and infrastructure engineering*, 17(12), 1626–1638.

Åström, K. J. and Wittenmark, B. (2013). *Computer-controlled systems: theory and design*. Courier Corporation.

Au, F., Cheng, Y., and Cheung, Y. (2001). "Vibration analysis of bridges under moving vehicles and trains: an overview." *Progress in Structural Engineering and Materials*, 3(3), 299–304.

Cheng, Y., Au, F., and Cheung, Y. (2001). "Vibration of railway bridges under a moving train by using bridge-track-vehicle element." *Engineering Structures*, 23(12), 1597–1606.

Craig Jr, R. R. and Kurdila, A. J. (2006). *Fundamentals of structural dynamics*. John Wiley & Sons.

Das, B. M. and Luo, Z. (2016). *Principles of soil dynamics*. Cengage Learning.

Di Lorenzo, S., Di Paola, M., Failla, G., and Pirrotta, A. (2017). "On the moving load problem in euler–bernoulli uniform beams with viscoelastic supports and joints." *Acta Mechanica*, 228(3), 805–821.

Dormand, J. R. and Prince, P. J. (1980). "A family of embedded runge-kutta formulae." *Journal of computational and applied mathematics*, 6(1), 19–26.

Feng, D. and Feng, M. Q. (2015). "Model updating of railway bridge using in situ dynamic displacement measurement under trainloads." *Journal of Bridge Engineering*, 20(12), 04015019.

Frỳba, L. (2013). *Vibration of solids and structures under moving loads*, Vol. 1. Springer Science & Business Media.

Gibbons, J. (1985). "Nonparametric statistical inference, 2nd edn. m." *Dekker, New York8. Groot P, ten Teije A, van Harmelen F (2004) A quantitative analysis of the robustness of knowledge-based systems through degradation studies. Knowl Inform Syst*, 7(2), 224245.

He, L., Castoro, C., Aloisio, A., Zhang, Z., Marano, G. C., Gregori, A., Deng, C., and Briseghella, B. (2021). "Dynamic assessment, fe modelling and parametric updating of a butterfly-arch stress-ribbon pedestrian bridge." *Structure and Infrastructure Engineering*, 1–12.

Hirzinger, B., Adam, C., and Salcher, P. (2020). "Dynamic response of a non-classically damped beam with general boundary conditions subjected to a moving mass-spring-damper system." *International Journal of Mechanical Sciences*, 185, 105877.

Ichikawa, M., Miyakawa, Y., and Matsuda, A. (2000). "Vibration analysis of the continuous beam

544 subjected to a moving mass." *Journal of Sound and Vibration*, 230(3), 493–506.

545 Ju, S.-H., Lin, H.-T., and Huang, J.-Y. (2009). "Dominant frequencies of train-induced vibrations."
546 *Journal of Sound and Vibration*, 319(1-2), 247–259.

547 Kathnelson, A. (1992). "High eigenfrequencies of non-uniform bernoulli-euler beams." *Interna-*
548 *tional journal of mechanical sciences*, 34(10), 805–808.

549 König, P., Salcher, P., Adam, C., and Hirzinger, B. (2021). "Dynamic analysis of railway bridges
550 exposed to high-speed trains considering the vehicle–track–bridge–soil interaction." *Acta Me-*
551 *chanica*, 232(11), 4583–4608.

552 Kumar, C. S., Sujatha, C., and Shankar, K. (2015). "Vibration of simply supported beams under
553 a single moving load: A detailed study of cancellation phenomenon." *International Journal of*
554 *Mechanical Sciences*, 99, 40–47.

555 Liu, K., De Roeck, G., and Lombaert, G. (2009). "The effect of dynamic train–bridge interaction on
556 the bridge response during a train passage." *Journal of sound and vibration*, 325(1-2), 240–251.

557 Majka, M. and Hartnett, M. (2008). "Effects of speed, load and damping on the dynamic response
558 of railway bridges and vehicles." *Computers & Structures*, 86(6), 556–572.

559 Mao, L. and Lu, Y. (2013). "Critical speed and resonance criteria of railway bridge response to
560 moving trains." *Journal of Bridge Engineering*, 18(2), 131–141.

561 Mottershead, J. E., Link, M., and Friswell, M. I. (2011). "The sensitivity method in finite element
562 model updating: A tutorial." *Mechanical systems and signal processing*, 25(7), 2275–2296.

563 Museros, P., Moliner, E., and Martínez-Rodrigo, M. D. (2013). "Free vibrations of simply-supported
564 beam bridges under moving loads: Maximum resonance, cancellation and resonant vertical
565 acceleration." *Journal of Sound and Vibration*, 332(2), 326–345.

566 Ouyang, H. (2011). "Moving-load dynamic problems: A tutorial (with a brief overview)." *Me-*
567 *chanical Systems and Signal Processing*, 25(6), 2039–2060.

568 Pasca, D. P., Aloisio, A., Fragiacomo, M., and Tomasi, R. (2021). "Dynamic characterization of
569 timber floor subassemblies: Sensitivity analysis and modeling issues." *Journal of Structural*
570 *Engineering*, 147(12), 05021008.

Peeters, B. and De Roeck, G. (2001). "Stochastic system identification for operational modal analysis: a review." *Journal of Dynamic Systems, Measurement, and Control*, 123(4), 659–667.

Pelliciari, M., Marano, G. C., Cuoghi, T., Briseghella, B., Lavorato, D., and Tarantino, A. M. (2018). "Parameter identification of degrading and pinched hysteretic systems using a modified bouc–wen model." *Structure and Infrastructure Engineering*, 14(12), 1573–1585.

Pesterev, A., Yang, B., Bergman, L., and Tan, C. (2003). "Revisiting the moving force problem." *Journal of sound and vibration*, 261(1), 75–91.

Rebelo, C., da Silva, L. S., Rigueiro, C., and Pircher, M. (2008). "Dynamic behaviour of twin single-span ballasted railway viaducts—field measurements and modal identification." *Engineering Structures*, 30(9), 2460–2469.

Rebelo, C., Heiden, M., Pircher, M., and Simões da Silva, L. (2005). "Vibration measurements on existing single-span concrete railway viaducts in austria." *Proc. of 6th International Conference on Structural Dynamics EURODY N*, Vol. 1637, 1642.

Reynders, E., Pintelon, R., and De Roeck, G. (2008). "Uncertainty bounds on modal parameters obtained from stochastic subspace identification." *Mechanical systems and signal processing*, 22(4), 948–969.

Ribeiro, D., Calçada, R., Delgado, R., Brehm, M., and Zabel, V. (2012). "Finite element model updating of a bowstring-arch railway bridge based on experimental modal parameters." *Engineering Structures*, 40, 413–435.

Robnett, Q., Thompson, M., Hay, W., Tayabji, S., and Knutson, R. (1975). "Technical data bases report. ballast and foundation materials research program." *Report no.*

Salcher, P. and Adam, C. (2015). "Modeling of dynamic train–bridge interaction in high-speed railways." *Acta Mechanica*, 226(8), 2473–2495.

Saltelli, A. and Sobol', I. M. (1995). "Sensitivity analysis for nonlinear mathematical models: numerical experience." *Matematicheskoe Modelirovanie*, 7(11), 16–28.

Selig, E. T. and Waters, J. M. (1994). *Track geotechnology and substructure management*. Thomas Telford.

598 Sirotti, S., Pelliciari, M., Di Trapani, F., Briseghella, B., Carlo Marano, G., Nuti, C., and Tarantino,
599 A. M. (2021). "Development and validation of new bouc–wen data-driven hysteresis model for
600 masonry infilled rc frames." *Journal of Engineering Mechanics*, 147(11), 04021092.
601 Svedholm, C., Zangeneh, A., Pacoste, C., François, S., and Karoumi, R. (2016). "Vibration of
602 damped uniform beams with general end conditions under moving loads." *Engineering Struc-*
603 *tures*, 126, 40–52.
604 Valle, J., Fernández, D., and Madrenas, J. (2019). "Closed-form equation for natural frequencies of
605 beams under full range of axial loads modeled with a spring-mass system." *International Journal*
606 *of Mechanical Sciences*, 153, 380–390.
607 Wu, Y.-S., Yang, Y.-B., and Yau, J.-D. (2001). "Three-dimensional analysis of train-rail-bridge
608 interaction problems." *Vehicle System Dynamics*, 36(1), 1–35.
609 Xia, H., Li, H., Guo, W., and De Roeck, G. (2014). "Vibration resonance and cancellation of
610 simply supported bridges under moving train loads." *Journal of Engineering Mechanics*, 140(5),
611 04014015.
612 Xia, H. and Zhang, N. (2005). "Dynamic analysis of railway bridge under high-speed trains."
613 *Computers & Structures*, 83(23-24), 1891–1901.
614 Xia, H., Zhang, N., and De Roeck, G. (2003). "Dynamic analysis of high speed railway bridge
615 under articulated trains." *Computers & Structures*, 81(26-27), 2467–2478.
616 Xia, H., Zhang, N., and Guo, W. (2018). "Dynamic interaction of train-bridge systems in high-speed
617 railways." *Springer, Berlin, Germany, DOI*, 10, 978–3.
618 Xu, Y. L., Zhang, N., and Xia, H. (2004). "Vibration of coupled train and cable-stayed bridge
619 systems in cross winds." *Engineering Structures*, 26(10), 1389–1406.
620 Yang, Y.-B., Yau, J., Yao, Z., and Wu, Y. (2004). *Vehicle-bridge interaction dynamics: with*
621 *applications to high-speed railways*. World Scientific.
622 Yang, Y.-B., Yau, J.-D., and Hsu, L.-C. (1997). "Vibration of simple beams due to trains moving
623 at high speeds." *Engineering structures*, 19(11), 936–944.
624 Zhai, W. et al. (2015). "Vehicle-track coupled dynamics." *Beijing: Science Press; Forthcoming*.

625 Zhai, W., Wang, S., Zhang, N., Gao, M., Xia, H., Cai, C., and Zhao, C. (2013). "High-speed train–
626 track–bridge dynamic interactions–part ii: experimental validation and engineering application."
627 *International Journal of Rail Transportation*, 1(1-2), 25–41.
628 Zhang, N., Xia, H., Guo, W., and De Roeck, G. (2010). "A vehicle–bridge linear interaction model
629 and its validation." *International Journal of Structural Stability and Dynamics*, 10(02), 335–361.
630 Zhang, Q.-L., Vrouwenvelder, A., and Wardenier, J. (2001). "Numerical simulation of train–bridge
631 interactive dynamics." *Computers & Structures*, 79(10), 1059–1075.
632 Zhu, Z., Gong, W., Wang, L., Li, Q., Bai, Y., Yu, Z., and Harik, I. E. (2018). "An efficient
633 multi-time-step method for train-track-bridge interaction." *Computers & Structures*, 196, 36–48.

APPENDIX I. FINITE DIFFERENCE FORMULATION

The $\boldsymbol{D}_4^{\{n\times n\}}$ matrix is four-banded matrix. The authors imposed the boundary conditions of a simply supported beam by replacing the coefficients in bold:

$$\boldsymbol{D}_4^{\{n\times n\}} = \frac{1}{\Delta x^4}\begin{bmatrix} \mathbf{4} & -4 & 1 & 0 & 0 & 0 & 0 & 0 & \vdots & 0 \\ \mathbf{-7/2} & 6 & -4 & 1 & 0 & 0 & 0 & 0 & \vdots & 0 \\ 1 & -4 & 6 & -4 & 1 & 0 & 0 & 0 & \vdots & 0 \\ 0 & 1 & -4 & 6 & -4 & 1 & 0 & 0 & \vdots & 0 \\ & & \ddots & \ddots & \ddots & \ddots & \ddots & & & \\ 0 & \vdots & 0 & 0 & 1 & -4 & 6 & -4 & 1 & 0 \\ 0 & \vdots & 0 & 0 & 0 & 1 & -4 & 6 & -4 & 1 \\ 0 & \vdots & 0 & 0 & 0 & 0 & 1 & -4 & -4 & \mathbf{-7/2} \\ 0 & \vdots & 0 & 0 & 0 & 0 & 0 & 1 & -4 & \mathbf{2} \end{bmatrix} \tag{30}$$

The bold coefficients yield a null bending moment and displacement in both the extremes of the beam.

List of Tables

TABLE 1. Optimum parameters of an equivalent EB beam model and comparison in terms of natural frequency and Modal Assurance Criterion (MAC).

Parameter	Value
f_{exp} [Hz]	8.61
f_{theo} [Hz]	8.62
MAC	0.92
$\frac{f_{\text{exp}}-f_{\text{theo}}}{f_{\text{exp}}}$ [%]	-0.12
$EI_{b,\text{opt}}$ [kN·mm^2]	12600

TABLE 2. List of the parameters chosen for the sensitivity analysis and range of variations.

Parameters	Label	lower bound	Upper bound	unit
Vertical stiffness of the ballast	k_f	6	600	Mpa
Damping coefficient of the ballast	c_f	0.1	100	Mpa s
Bending stiffness of the bridge	$E_c I_c$	$(1-50\%)EI_{b,\text{opt}}$	$(1+50\%)EI_{b,\text{opt}}$	kN/mm^2
Velocity of the train	c	50	200	km/h

TABLE 3. Input parameters of the optimization algorithm.

Input parameters			
Description	Label	Value	Unit
Beam length	L	19.85	m
Discretization step	Δx	0.5	m
Concrete specific mass	ρ_c	2500	kg/m^3
Cross-section area of the bridge	A_c	6.67	m^2
Ballast specific mass	ρ_b	2000	kg/m^3
Cross-section area of the rails	A_r	0.01	m2
Steel specific mass	ρ_s	2000	kg/m^3
Cross-section area of the ballast	A_b	5.67	m^2
Bending stiffness of the bridge	$E_c I_c$	12600	kN·mm^2
Young's modulus of steel	E_s	210000	Mpa
Cross section area of the rails	I_r	$833{\cdot}10^4$	mm^4
Velocity of the train	c	110	km/h
Locomotive's length	L_v	5	m
Car's length	L_v	22	m
Locomotive weight	P_l	300	kN
Car's weight	P_c	600	kN
Number of locomotives		2	
Number of cars		7	

TABLE 4. Results of the sensitivity analysis.

Parameters	Peak displacement		Rank correlation coefficient	
Sensitivity indicators	S_1 [%]	S_T [%]	S_1 [%]	S_T [%]
Vertical stiffness of the ballast	38.56	41.34	39.72	39.61
Damping coefficient of the ballast	20.31	22.34	33.65	34.67
Bending stiffness of the bridge	40.26	45.12	38.23	39.34
Velocity of the train	0.89	1.23	/	/
Sum	100.02	110.03	111.6	113.62

List of Figures

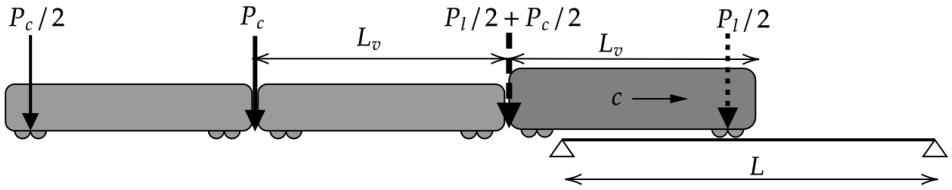

Fig. 1. Illustration of train load model using concentrated forces.

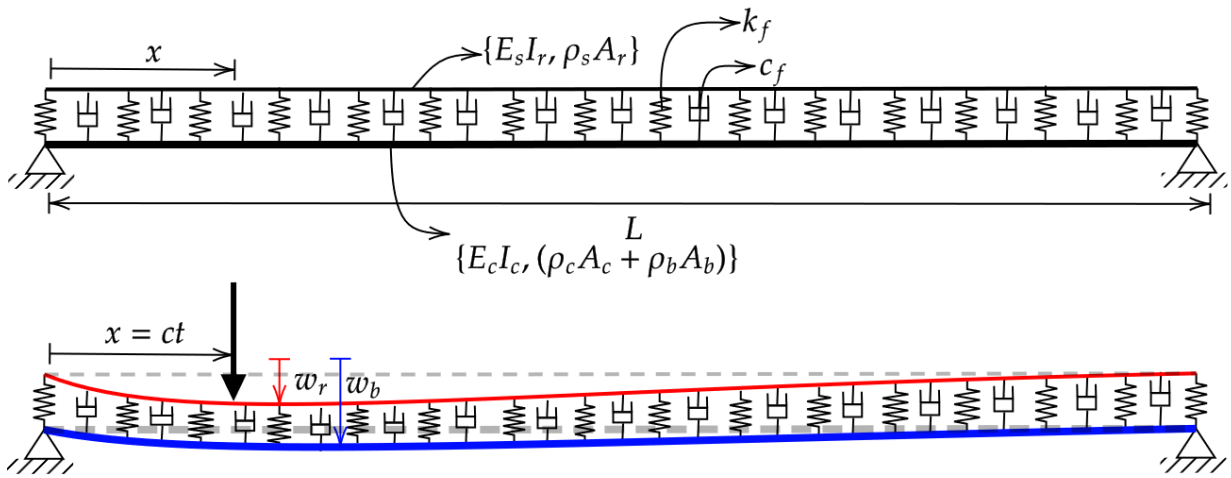

Fig. 2. Illustration of the mathematical model of the TTBI.

Fig. 3. Views of the viaduct and of a sample span.

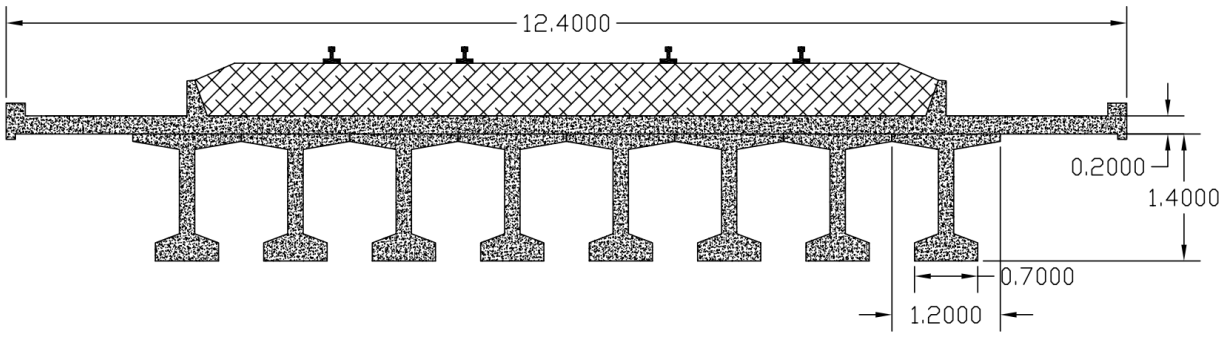

Fig. 4. Cross-section of the Orte-Falconara bridge. The dimensions are in meters.

Fig. 5. View of the experimental setup of the Orte-Falconara bridge (1st case study).

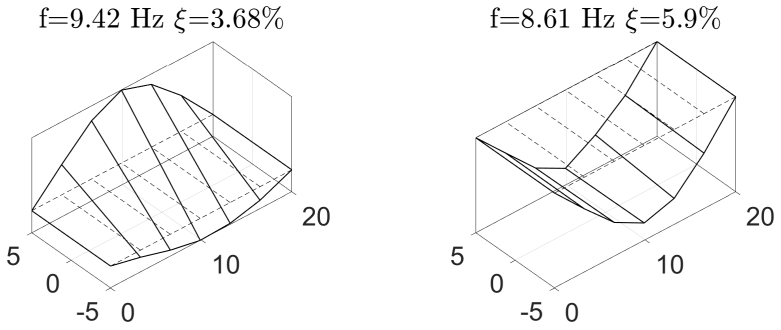

Fig. 6. Experimental mode shapes of the first two stable modes.

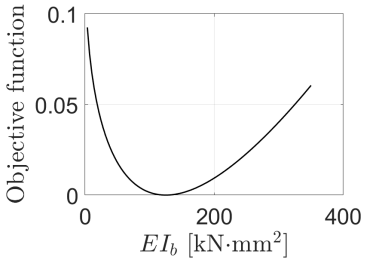

Fig. 7. Objective function in Eq.18

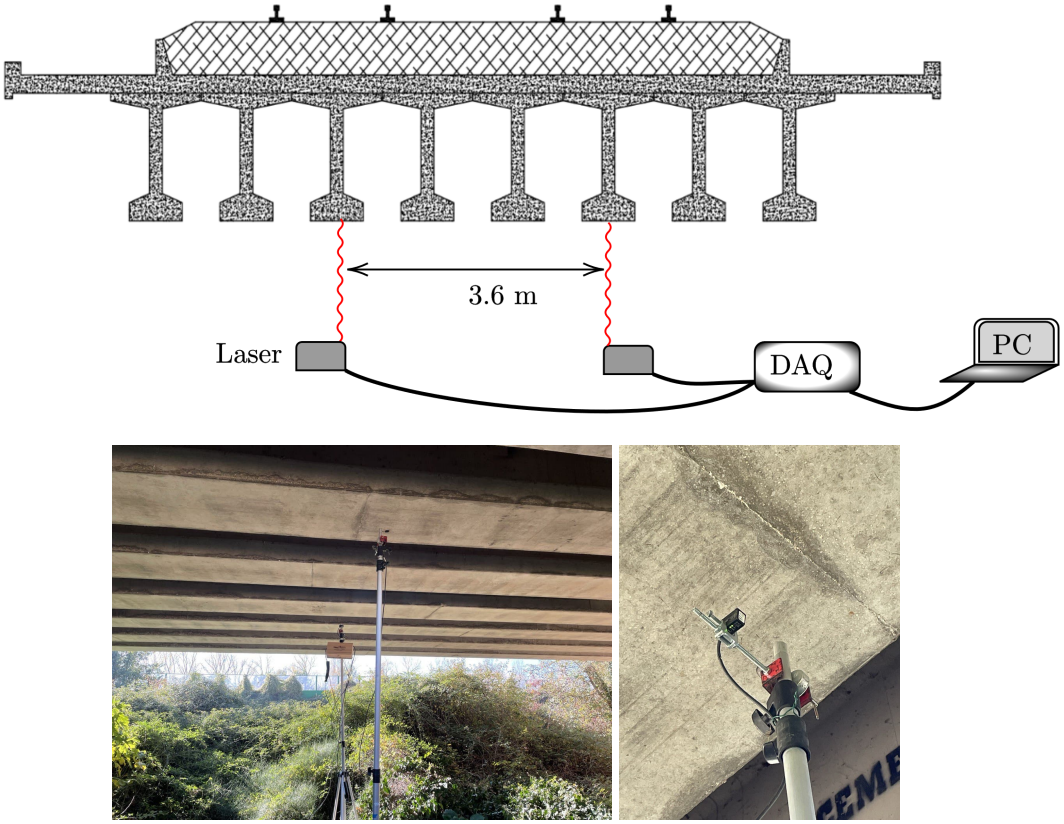

Fig. 8. View of the sensors layout and experimental setup in the Orte-Falconara bridge (1st case study) for the bridge deflection measurement using laser sensors under the train transit.

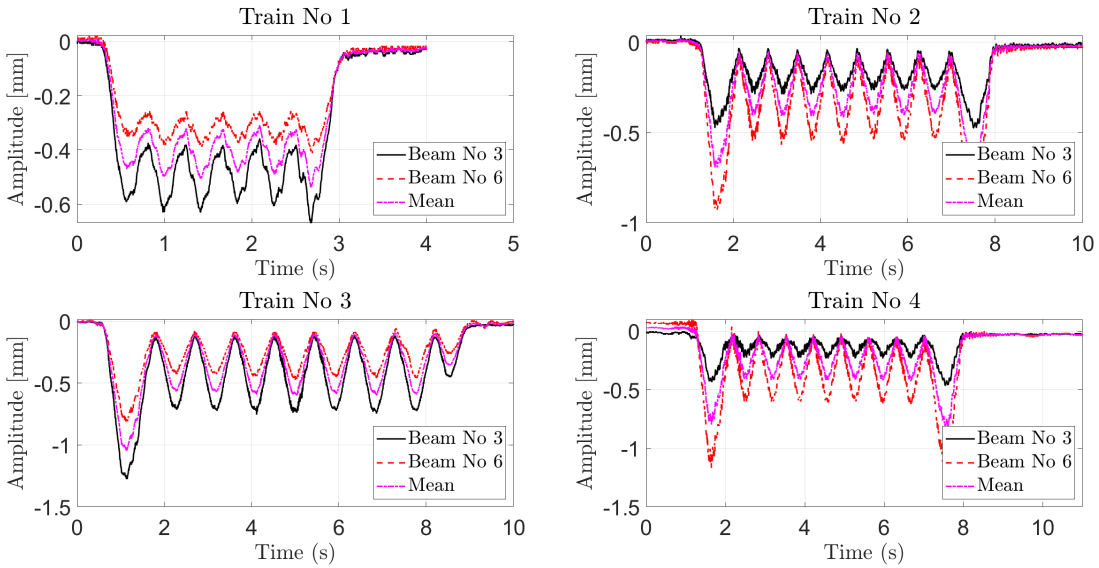

Fig. 9. Displacement response of the bridge under four moving trains.

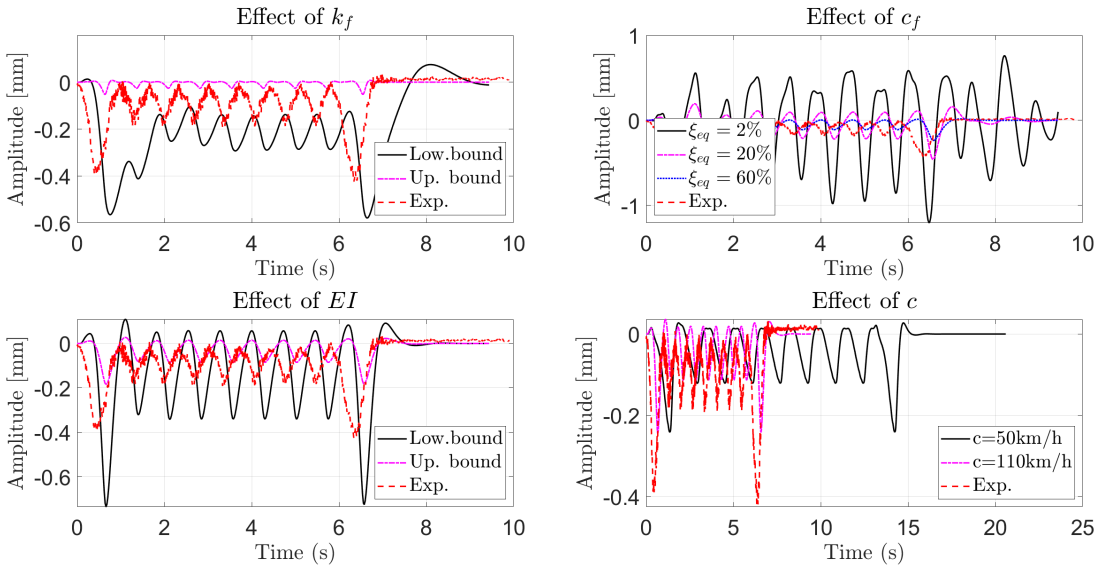

Fig. 10. Monovariate sensitivity analyses.

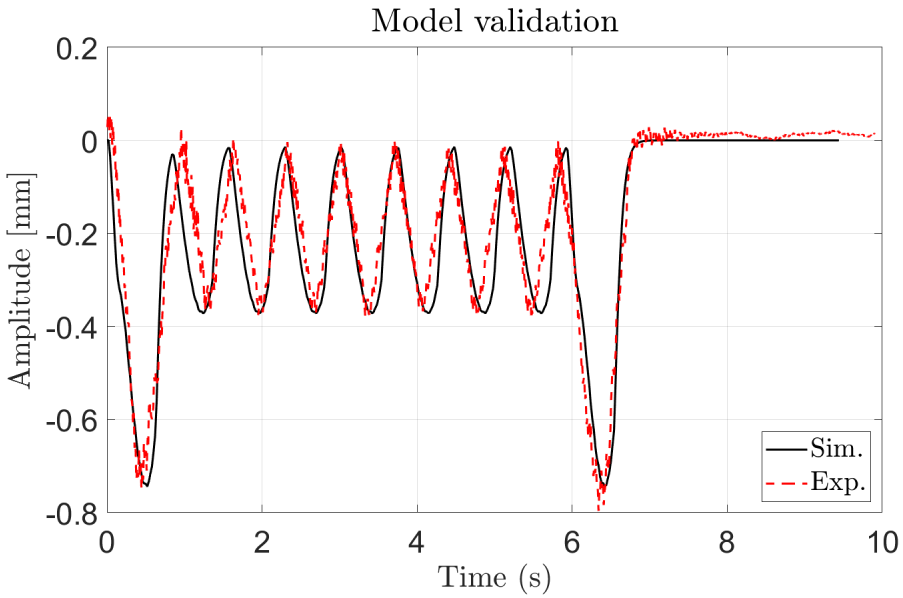

Fig. 11. Comparison between the experimental and simulated displacement response obtained with the optimized parameters.

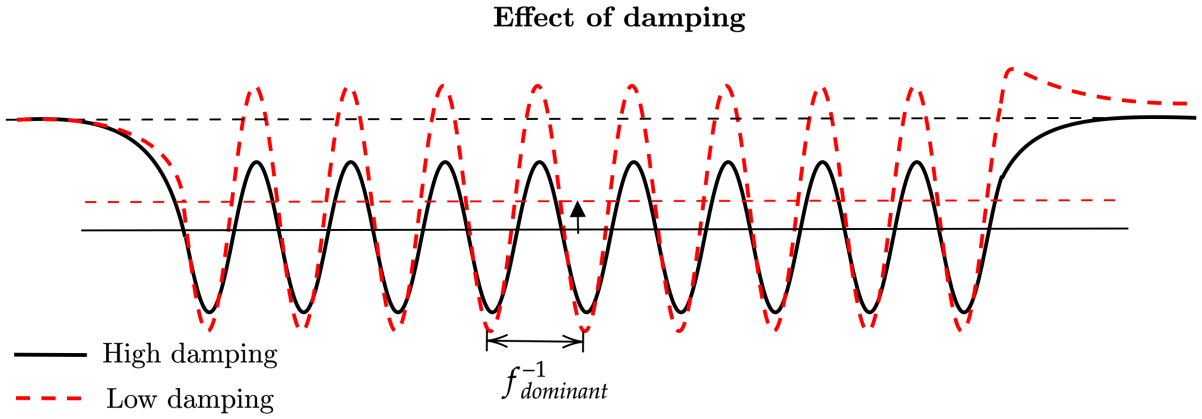

Fig. 12. Illustration of the damping effects.

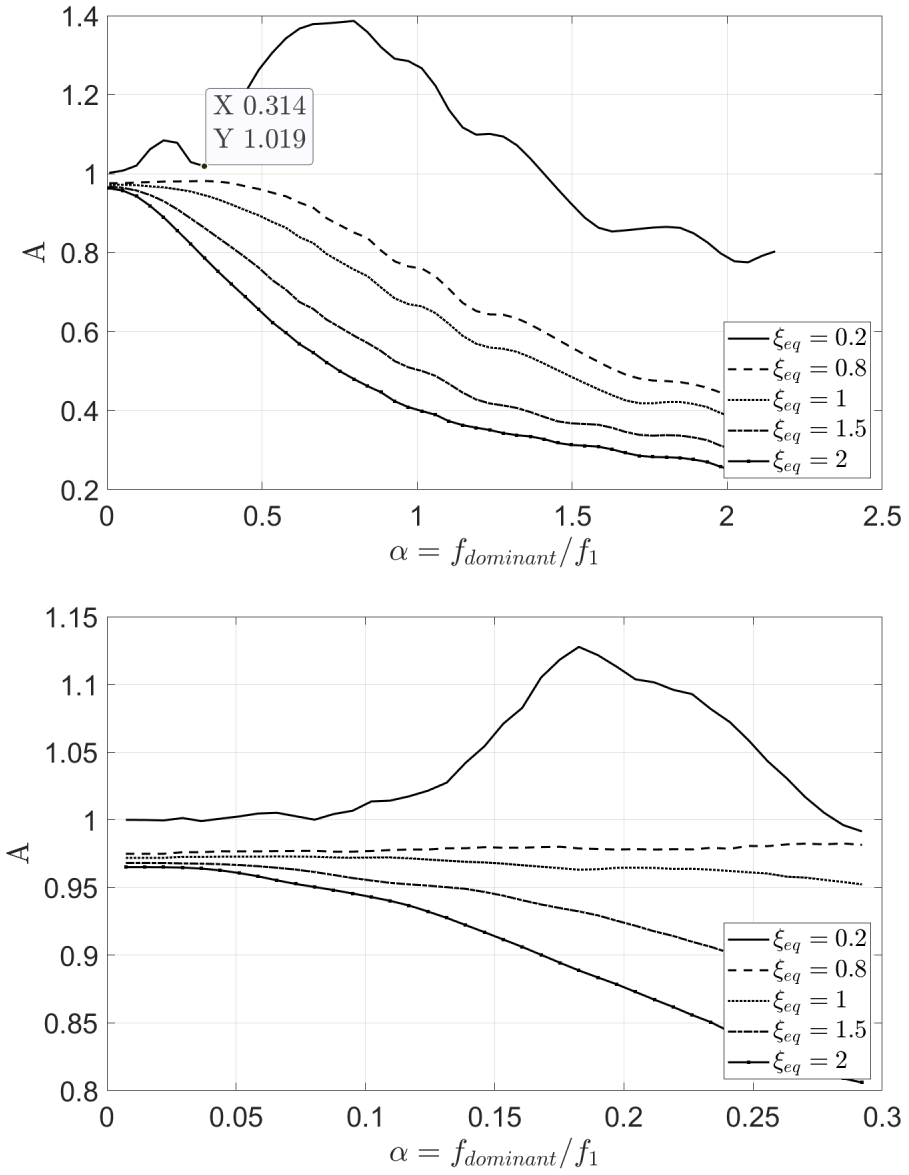

Fig. 13. Effect of the train velocity, where $f_{\text{dominant}} = c/L_v$, and $f_1 = 8.61$Hz.